Automatica 125 (2021) 109381

Contents lists available at ScienceDirect

Automatica

journal homepage: www.elsevier.com/locate/automatica

Brief paper

Stop-and-go suppression in two-class congested traffic☆

Mark Burkhardt [a], Huan Yu [b,*], Miroslav Krstic [b]

[a] Institute for System Dynamics, University of Stuttgart, Waldburgst. 17/19, Stuttgart, 70563, Germany
[b] Department of Mechanical and Aerospace Engineering, University of California, San Diego, La Jolla, CA, 92093, USA

ARTICLE INFO

Article history:
Received 15 May 2019
Received in revised form 14 July 2020
Accepted 14 November 2020
Available online xxxx

Keywords:
Multi-class traffic model
PDE control
Backstepping
Output feedback controller

ABSTRACT

This paper develops an output feedback control law in order to damp out traffic oscillations in the congested regime of the linearized two-class Aw-Rascle (AR) traffic model. The macroscopic second-order two-class AR traffic model consists of four hyperbolic partial differential equations (PDEs) describing the dynamics of densities and velocities on freeway. Each vehicle class is characterized by its own vehicle size and driver's behavior. The considered equilibrium profiles of the model represent evenly distributed traffic with constant densities and velocities of both classes along the investigated track section. After linearizing the model equations around those equilibrium profiles, it is observed that in the congested traffic one of the four characteristic speeds is negative, whereas the remaining three are positive. Backstepping control design is employed to stabilize the 4×4 heterodirectional hyperbolic PDEs. The control input actuates the traffic flow at outlet of the investigated track section and is realized by a ramp metering. The output feedback controller is obtained by designing an anti-collocated observer and combining it with a full state feedback result. Overall, the output feedback control law achieves the damping of stop-and-go waves in finite time by measuring the velocities and densities of both vehicle classes at the inlet of the investigated track section. The performance of the developed controller is verified by simulation of the linearized model and quantified by performance indices for the fuel consumption, comfort and total travel time.

1. Introduction

Nowadays, more and more people own a car leading to crowded highways and congested traffic during rush hours in many countries of the world. Stop-and-go traffic is common to appear in congested traffic. This phenomenon is characterized by traffic density and velocity perturbations, causing higher fuel consumption and a higher risk of accidents. The overall challenge addressed in this work is the design of a ramp metering traffic management system to reduce traffic oscillations in the congested regime while distinguishing two different vehicle classes. Thereby, a vehicle class is defined to be a group of vehicles with the same properties, see Logghe (2003).

In general, traffic models are categorized in micro-, meso- and macroscopic models. Macroscopic models describe the traffic as a continuum and are thus more suitable to investigate traffic jams and disturbances in traffic flow. Typically, their model equations are PDEs. Macroscopic second-order multi-class models are introduced in, Gupta and Katiyar (2007), Jiang and Wu (2004), Mohan and Ramadurai (2017), Tang, Huang, Zhao, and Shang (2009) and Tang, Jiang, Wu, Wiwatanapataphee, and Wu (2007). The denoted second-order models differ in the terms that occur in the velocity dynamics and in the principles which are used to deduce them. The main focus of this paper is the macroscopic multi-class model (Mohan & Ramadurai, 2017), because it is validated by simulation and compared to other macroscopic multi-class models as well as considers the size of vehicles. For the case of two different classes, this extension of the AR traffic model yields four coupled nonlinear hyperbolic PDEs which are denoted as the two-class AR traffic model in the following. In order to consider vehicle sizes, the vehicles are assumed to adjust their speed according to a measure called area occupancy which needs to be distinguished from occupancy (Mallikarjuna & Rao, 2006).

Controllers for traffic models are developed in Bekiaris-Liberis and Delis (2019) and Karafyllis, Bekiaris-Liberis, and Papageorgiou (2019) focusing on the stabilization of equilibria. Whereas the control input of Bekiaris-Liberis and Delis (2019) is given by Adaptive Cruise Control-equipped vehicles yielding in-domain actuation, Karafyllis et al. (2019) develop a boundary feedback law for the inlet demand. In Pasquale et al. (2015), an algorithm solving a multi-objective optimal control problem is presented

☆ The material in this paper was partially presented at the 21st IFAC World Congress (IFAC 2020), July 12–17, 2020, Berlin, Germany. This paper was recommended for publication in revised form by Associate Editor Antonella Ferrara under the direction of Editor Thomas Parisini.

* Corresponding author.
E-mail addresses: burkhardt@isys.uni-stuttgart.de (M. Burkhardt), huy015@ucsd.edu (H. Yu), krstic@ucsd.edu (M. Krstic).

https://doi.org/10.1016/j.automatica.2020.109381
0005-1098/

in a multi-class traffic framework considering two classes. The optimization aims to minimize an objective function including total emission and total time spent. Moreover, Deo, De Schutter, and Hegyi (2009) present a Model Predictive Control approach to coordinate traffic management systems like ramp metering and variable speed limits for a multi-class traffic flow model. The cost functional employed in the presented benchmark example is the total time spent by the vehicles in the network. Additionally, Liu, Hellendoorn, and De Schutter (2017) also apply a Model Predictive Control Approach based on multi-class emission and traffic flow models considering the total time spent and total emission with variable speed limits and ramp metering as control measures. Typically, traffic management systems act on the boundary of the investigated track section yielding a boundary control problem. Further efforts focused on boundary control of stop-and-go traffic with traffic management systems are given by Burkhardt, Yu, and Krstic (2020), Yu and Krstic (2018, 2019) and Zhang and Prieur (2017).

In literature, different techniques are proposed that achieve convergence of the states of hyperbolic coupled PDEs to a constant equilibrium with boundary control. The main focus of this paper is on the backstepping stabilization technique (Deutscher, 2017; Hu, Meglio, Vazquez, & Krstic, 2015; Meglio, Vazquez, & Krstic, 2013; Su, Wang, & Krstic, 2017). In fact, the presented output feedback control of this work is based on the full state feedback result of Burkhardt et al. (2020) and corresponds to the special case of the theoretical result in Hu et al. (2015) where three transport systems propagate downstream and one transport system propagates upstream.

Contribution: this work presents the first result on output feedback boundary control design with backstepping for traffic congestion consisting of two different vehicle classes. On one hand, this work contributes to traffic modeling in the sense of deducing a macroscopic multi-class traffic model in its characteristic form and investigating the obtained characteristic speeds. On the other hand, the theoretical control design method backstepping is applied to an up-to-date extension of the AR traffic model for two classes is created by designing an output feedback controller as ramp metering signal.

This paper is structured as follows: Section 2 introduces the two-class AR traffic model, the parameters characterizing the two classes and the formulation of the control design model. Furthermore, the output feedback controller result is presented in Section 3. Section 4 verifies the performance of the presented controller with simulation results obtained by the linearized model and covers the computation of performance indices. Future work is discussed in Section 5.

2. Problem statement

The two-class AR traffic model is presented and important model parameters are explained. Afterwards, the model equations are linearized around a constant equilibrium, followed by a discussion of boundary conditions, its qualitative behavior in the congested regime and a transformation to Riemann coordinates in order to obtain the control design model.

2.1. Two-class AR traffic model

The extended AR model for heterogeneous traffic presented in Mohan and Ramadurai (2017) is investigated in case of two classes and is then given by

$$\partial_t \rho_1 = -\partial_x(\rho_1 v_1), \tag{1a}$$

$$\partial_t(v_1 + p_1(AO)) + v_1\partial_x(v_1 + p_1(AO)) = \frac{V_{e,1}(AO) - v_1}{\tau_1}, \tag{1b}$$

$$\partial_t \rho_2 = -\partial_x(\rho_2 v_2), \tag{1c}$$

$$\partial_t(v_2 + p_2(AO)) + v_2\partial_x(v_2 + p_2(AO)) = \frac{V_{e,2}(AO) - v_2}{\tau_2}, \tag{1d}$$

where each vehicle class i is described by traffic density $\rho_i(x,t)$ and velocity $v_i(x,t)$ with $(x,t) \in (0,L)\times(0,\infty)$. The corresponding initial conditions are $\rho_i(x,0) = \rho_{i,0}(x) \in \mathscr{L}^\infty([0,L])$ and $v_i(x,0) = v_{i,0}(x) \in \mathscr{L}^\infty([0,L])$. Additionally, the boundary conditions (11) are motivated and discussed in Section 2.3. The parameter L is the length of the investigated track section. The traffic density $\rho_i(x,t)$ is defined as vehicles per unit length. In addition, the velocity $v_i(x,t)$ describes the velocity at a specified spatial point along the investigated track section. Moreover, τ_i is the so-called adaptation time. The variable $AO(\rho_1,\rho_2)$ describes the area occupancy and is based on the definition of the occupancy introduced (Mallikarjuna & Rao, 2006). In Mohan and Ramadurai (2017), the expression for the area occupancy is simplified to

$$AO(\rho_1,\rho_2) = \frac{a_1 L\rho_1 + a_2 L\rho_2}{WL}, \tag{2}$$

where a_i is the occupied surface and W the width of the investigated track. Area occupancy AO describes the percentage of road space that is occupied if vehicles of class one are distributed with density $\rho_1(x,t)$ and vehicles of class two are distributed with density $\rho_2(x,t)$ along the considered track section. The traffic pressure function $p_i(AO)$ is formulated as

$$p_i(AO) = V_i\left(\frac{AO(\rho_1,\rho_2)}{\overline{AO}_i}\right)^{\gamma_i}, \tag{3}$$

and the equilibrium speed-AO relationship $V_{e,i}(AO)$ as

$$V_{e,i}(AO) = V_i\left(1 - \left(\frac{AO(\rho_1,\rho_2)}{\overline{AO}_i}\right)^{\gamma_i}\right), \tag{4}$$

according to the model of Greenshield (Greenshields, Channing, & Miller, 1935). The experienced traffic pressure $p_i(AO)$ grows with AO. The equilibrium speed-AO relationship $V_{e,i}(AO)$ describes the desired velocity of the drivers. More crowded freeways lead to higher AO and therefore a lower desired velocity. Therein, V_i corresponds to the free-flow velocity, $\gamma_i > 1$ to the traffic pressure exponent and $\overline{AO}_i$ to the maximum area occupancy. The free-flow velocity V_i represents the desired velocity of a driver, if no other vehicles of any class are present, $V_{e,i}(0) = V_i$. The pressure exponent γ_i is a degree of freedom to model the experienced traffic pressure of the drivers correctly. The maximum area occupancy $\overline{AO}_i$ describes the percentage of occupied road surface for which the corresponding vehicle class is jammed, i.e. $V_{e,i}(\overline{AO}_i) = 0$. To obtain physically meaningful results, $0 < \overline{AO} \leq 1$ holds.

2.2. Linearized two-class AR traffic model

The two-class AR traffic model (1) is linearized around a constant equilibrium $z^* = (\rho_1^*, v_1^*, \rho_2^*, v_2^*)^T$. Inserting this constant state in (1) yields the conditions

$$v_i^*(\rho_1^*,\rho_2^*) = V_{e,i}(AO(\rho_1^*,\rho_2^*)). \tag{5}$$

Thus, the equilibrium velocities are determined by the equilibrium densities ρ_1^* and ρ_2^*. The perturbations of the distributed variables $\rho_i(x,t)$ and $v_i(x,t)$ are defined as

$$\tilde{\rho}_i(x,t) = \rho_i(x,t) - \rho_i^*, \quad \tilde{v}_i(x,t) = v_i(x,t) - v_i^*, \tag{6}$$

and the linearized model equations are given by

$$J_t z_t + J_x z_x + Jz = 0, \tag{7}$$

with state vector $z = (\tilde{\rho}_1, \tilde{v}_1, \tilde{\rho}_2, \tilde{v}_2)^T$ and where the introduced Jacobian matrices are

$$J_t = \begin{bmatrix} 1 & 0 & 0 & 0 \\ \beta_{11} & 1 & \beta_{12} & 0 \\ 0 & 0 & 1 & 0 \\ \beta_{21} & 0 & \beta_{22} & 1 \end{bmatrix}, \; J_x = \begin{bmatrix} v_1^* & \rho_1^* & 0 & 0 \\ v_1^*\beta_{11} & v_1^* & v_1^*\beta_{12} & 0 \\ 0 & 0 & v_2^* & \rho_2^* \\ v_2^*\beta_{21} & 0 & v_2^*\beta_{22} & v_2^* \end{bmatrix},$$

$$J = \begin{bmatrix} 0 & 0 & 0 & 0 \\ \frac{1}{\tau_1}\beta_{11} & \frac{1}{\tau_1} & \frac{1}{\tau_1}\beta_{12} & 0 \\ 0 & 0 & 0 & 0 \\ \frac{1}{\tau_2}\beta_{21} & 0 & \frac{1}{\tau_2}\beta_{22} & \frac{1}{\tau_2} \end{bmatrix} \tag{8}$$

including the abbreviation

$$\beta_{ij}(\rho_1^*, \rho_2^*) = \left. \frac{\partial p_i(AO(\rho_1, \rho_2))}{\partial \rho_j} \right|_{\rho_1=\rho_1^*, \rho_2=\rho_2^*} \tag{9}$$

with $i, j = 1, 2$.

2.3. Boundary conditions

The boundary conditions are motivated by a short time period consideration of the track section. Based on averaging over this short time frame at the boundaries, it is assumed that the same total traffic flow enters and leaves the track section which is given by the sum of the class 1 and class 2 equilibrium flows. Moreover, the traffic densities of the incoming traffic flow are equivalent to the equilibrium densities. Notice that the traffic flow $q_i(x, t)$ is given by the product of density and velocity of a class, i.e. $q_i(x, t) = \rho_i(x, t)v_i(x, t)$. It describes the amount of vehicles passing a spatial point x in a unit time frame. In addition, ramp metering is considered to be installed at the outlet of the investigated track section. Consequently, the traffic flow at the outlet is obtained by adding the traffic flow of the mainline and the traffic flow of the ramp, i.e.

$$q_1(L, t) + q_2(L, t) = q_{\text{mainline}}(L, t) + q_{\text{ramp}}(L, t). \tag{10}$$

Regarding $q_{\text{ramp}}(L, t)$, it is assumed that a constant entering traffic flow q_{in}^* is present on the ramp. Then, the control input is defined as the deviation of q_{in}^* yielding $q_{\text{ramp}}(L, t) = q_{in}^* + U(t)$. Due to the short time period consideration, the sum of traffic flow of the mainline and the constant entering traffic flow of the ramp is given by sum of the equilibrium traffic flows for each class, i.e. $q_{\text{mainline}}(L, t) + q_{in}^* = q_1^* + q_2^*$. Briefly summarized, this yields the boundary conditions

$$\rho_i(0, t) = \rho_i^*, \; q_1(0, t) + q_2(0, t) = \rho_1^* v_1^* + \rho_2^* v_2^*, \tag{11a}$$

$$q_1(L, t) + q_2(L, t) = \rho_1^* v_1^* + \rho_2^* v_2^* + U(t) \tag{11b}$$

and the corresponding linearized boundary conditions

$$0 = \tilde{\rho}_i(0, t), \tag{12a}$$

$$0 = v_1^*\tilde{\rho}_1(0, t) + \rho_1^*\tilde{v}_1(0, t) + v_2^*\tilde{\rho}_2(0, t) + \rho_2^*\tilde{v}_2(0, t), \tag{12b}$$

$$U(t) = v_1^*\tilde{\rho}_1(L, t) + \rho_1^*\tilde{v}_1(L, t) + v_2^*\tilde{\rho}_2(L, t) + \rho_2^*\tilde{v}_2(L, t). \tag{12c}$$

2.4. Congested regime analysis

In general, two different regimes of traffic are distinguished: the free-flow regime and the congested regime. A partial upstream propagation of information characterizes the traffic flow in the congested regime. The corresponding heterodirectional behavior causes the development of stop-and-go traffic implying increased fuel consumption and risk of accidents. In the following, the qualitative behavior of the linearized model (7) and (12) in the congested regime is investigated by considering the signs of the characteristic speeds. Notice that a negative characteristic speed indicates information propagating upstream. Decoupling in time derivatives and determining the eigenvalues of the resulting Jacobian that is multiplied with the spatial derivatives of the density and velocity perturbations afterwards, yields the characteristic speeds

$$\lambda_i = v_i^*, \; i = 1, 2, \quad \lambda_{3/4} = \frac{v_1^* + v_2^* - \beta_{11}\rho_1^* - \beta_{22}\rho_2^* \pm \Delta}{2}, \tag{13}$$

where

$$\Delta(\rho_1^*, \rho_2^*) = \sqrt{\left(\beta_{22}\rho_2^* - \beta_{11}\rho_1^* + v_1^* - v_2^*\right)^2 + 4\beta_{11}\beta_{22}\rho_1^*\rho_2^*}. \tag{14}$$

For model validity, the equilibrium velocities of both vehicle classes are chosen to be positive, i.e. $v_1^* > 0$ and $v_2^* > 0$ since all vehicles travel downstream. Thus, the first two characteristic speeds λ_1 and λ_2 are positive. In addition, it is shown in Zhang, Liu, Wong, and Dai (2006) that

$$\lambda_4 \leq \min\{\lambda_1, \lambda_2\} \leq \lambda_3 \leq \max\{\lambda_1, \lambda_2\} \tag{15}$$

holds. Hence, the only characteristic speed that may have a negative sign is λ_4. Therefore, traffic is defined to be in the congested regime if the equilibrium and parameters that determine the characteristic speeds satisfy $\lambda_1, \lambda_2, \lambda_3 > 0$ and $\lambda_4 < 0$. Since a controller dealing with congested traffic is designed later on, it is assumed that the equilibrium densities and parameters are chosen such that the presented inequalities hold throughout the rest of this paper.

2.5. Transformation to Riemann coordinates

The system is transformed to Riemann coordinates in order to obtain the control design model. The control design model variables are denoted by $w_c = (w_1, w_2, w_3, w_4)^T$. To keep the computations concise, the first three variables are summarized in $w = (w_1, w_2, w_3)^T$. The transformation achieves zero elements on the diagonal of the coefficient matrix occurring in the source term and sorts the positive characteristic speeds λ_1, λ_2 ad λ_3 in ascending order on the diagonal of the coefficient matrix of the spatial derivatives. Thus, the notation of Hu et al. (2015) can be adapted to increase the readability and the computations are more concise. In the following, it is assumed that class 1 vehicles represent small and fast average vehicles whereas class 2 describes big trucks which are large and slow. Thus, for the equilibrium velocities $v_1^* > v_2^*$ holds and therefore the ascending order of positive characteristic speeds is $\lambda_2 < \lambda_3 < \lambda_1$. The state transformation is defined as

$$w_c = \begin{bmatrix} 0 & e^{-\frac{\hat{J}_{22}}{v_2^*}x} & 0 & 0 \\ 0 & 0 & e^{-\frac{\hat{J}_{33}}{\lambda_3}x} & 0 \\ e^{-\frac{\hat{J}_{11}}{v_1^*}x} & 0 & 0 & 0 \\ 0 & 0 & 0 & e^{-\frac{\hat{J}_{44}}{\lambda_4}x} \end{bmatrix} \Theta^{-1} z \tag{16}$$

where the constant invertible transformation matrix Θ satisfies

$$\text{diag}(\lambda_1, \lambda_2, \lambda_3, \lambda_4) = \Theta^{-1} J_t^{-1} J_x \Theta \tag{17}$$

and therefore diagonalizes the Jacobian $J_t^{-1}J_x$. The entries of Θ are denoted as $\Theta = \{\theta_{ij}\}_{1\leq i\leq 4, 1\leq j\leq 4}$ and are straightforward to obtain but omitted in this paper due to their complexity and length. In addition, the constants $\{\hat{J}_{ij}\}_{1\leq i\leq 4, 1\leq j\leq 4}$ represent the entries of the matrix $\hat{J} = -\Theta^{-1}J_t^{-1}J\Theta$. The transformed model equations are given by

$$w_t + \Lambda^+ w_x = \Sigma^{++}(x)w + \Sigma^{+-}(x)w_4, \tag{18a}$$

$$w_{4t} - \Lambda^- w_{4x} = \Sigma^{-+}(x)w \tag{18b}$$

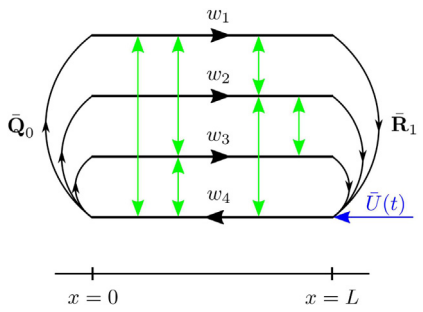

Fig. 1. Schematic diagram of the control design model. The green arrows represent the couplings between the states. The blue arrow indicates the location at which the control input acts on the system.

with

$$\Lambda^+ = \mathrm{diag}(v_2^*, \lambda_3, v_1^*), \quad \Lambda^- = -\lambda_4, \tag{19}$$

$$\Sigma^{++}(x) = \begin{bmatrix} 0 & \bar{J}_{12}(x) & \bar{J}_{13}(x) \\ \bar{J}_{21}(x) & 0 & \bar{J}_{23}(x) \\ \bar{J}_{31}(x) & \bar{J}_{32}(x) & 0 \end{bmatrix}, \tag{20}$$

$$\Sigma^{+-}(x) = \begin{bmatrix} \bar{J}_{14}(x) & \bar{J}_{24}(x) & \bar{J}_{34}(x) \end{bmatrix}^T, \tag{21}$$

$$\Sigma^{-+}(x) = \begin{bmatrix} \bar{J}_{41}(x) & \bar{J}_{42}(x) & \bar{J}_{43}(x) \end{bmatrix}. \tag{22}$$

The abbreviations for the coefficients of the source term, $\bar{J}_{ij}(x)$, $i, j = 1, \ldots, 4$, are not stated here due to space constraints. However, it is important to mention that $\bar{J}_{ij}(x)$ are bounded and either positive or negative on the whole domain of x. Applying the transformation to the boundary conditions (12) yields

$$w(0, t) = \bar{Q}_0 w_4(0, t), \tag{23a}$$

$$w_4(L, t) = \bar{R}_1 w(L, t) + \bar{U}(t) \tag{23b}$$

where the matrices

$$\bar{Q}_0 = -\begin{bmatrix} \theta_{12} & \theta_{13} & \theta_{11} \\ \theta_{32} & \theta_{33} & \theta_{31} \\ \kappa_2 & \kappa_3 & \kappa_1 \end{bmatrix}^{-1} \begin{bmatrix} \theta_{14} \\ \theta_{34} \\ \kappa_4 \end{bmatrix}, \tag{24a}$$

$$\bar{R}_1 = -\begin{bmatrix} \frac{\kappa_2}{\kappa_4} e^{\left(\frac{\hat{J}_{22}}{v_2^*} - \frac{\hat{J}_{44}}{\lambda_4}\right)L} & \frac{\kappa_3}{\kappa_4} e^{\left(\frac{\hat{J}_{33}}{\lambda_3} - \frac{\hat{J}_{44}}{\lambda_4}\right)L} & \frac{\kappa_1}{\kappa_4} e^{\left(\frac{\hat{J}_{11}}{\lambda_1} - \frac{\hat{J}_{44}}{\lambda_4}\right)L} \end{bmatrix} \tag{24b}$$

are obtained by formulating the linearized boundary conditions in matrix form, inserting the transformation law (16) and decoupling afterwards. Therein, the abbreviation $\kappa_j = v_1^* \theta_{1j} + \rho_1^* \theta_{2j} + v_2^* \theta_{3j} + \rho_2^* \theta_{4j}$, $j = 1, \ldots, 4$ is introduced. All numerical investigations that were performed while carrying out this work show that $\kappa_4 \neq 0$ if $v_1^*, v_2^* > 0$. In addition, the transformed input $\bar{U}(t)$ satisfies

$$\bar{U}(t) = e^{-\frac{\hat{J}_{44}}{\lambda_4} L} \frac{1}{\kappa_4} U(t). \tag{25}$$

Briefly summarized, the control design model is given by (18) and (23). Since the transformation (16) is invertible, the stability properties of the linearized model in density and velocity perturbations and the control design model are the same. In Fig. 1, the qualitative behavior of the control design model is illustrated. According to the sign of the characteristic speeds, the propagation direction for each state $w_j(x, t)$ is drawn in Fig. 1. It shows that the control input $\bar{U}(t)$ acts at the outlet of the system, first propagating upstream and, after it is carried through the boundary condition at the inlet of the investigated track section, affecting downstream traffic.

3. Output feedback control design

The output feedback controller is designed by combining the full-state feedback result of Burkhardt et al. (2020) with an anti-collocated observer based on Hu et al. (2015). The overall goal is to damp out stop-and-go traffic in the congested regime and achieve convergence to the equilibrium in a finite time for initial conditions $w_j(x, 0) \in \mathscr{L}^\infty[0, L]$. The resulting control law represents the main result of this work and is stated in a theorem.

3.1. Full-state feedback control result

The full-state feedback control law

$$U(t) = -\kappa_4 e^{\frac{\hat{J}_{44}}{\lambda_4} L} \bar{R}_1 T_u^{-1}(L) z(L, t) + \kappa_4 e^{\frac{\hat{J}_{44}}{\lambda_4} L} \int_0^L \left(K(L, \xi) T_u^{-1}(\xi) + L_{11}(L, \xi) T_l^{-1}(\xi) \right) z(\xi, t) d\xi \tag{26}$$

is developed in Burkhardt et al. (2020) and computed with the help of the backstepping technique. Therein, the kernels $K(x, \xi)$ and $L_{11}(x, \xi)$ are defined on the triangular domain $\mathscr{T} = \{0 \leq \xi \leq x \leq 1\}$. The kernel $K(x, \xi)$ is obtained by solving the well-posed kernel equations

$$\begin{aligned} 0 =& \lambda_4 K_x(x, \xi) + \Lambda^+ K_\xi(x, \xi) + K(x, \xi) \Sigma^{++}(\xi) \\ & - \frac{1}{\lambda_4} K(x - \xi, 0) \Lambda^+ \bar{Q}_0 \Sigma^{-+}(\xi) \\ & + \int_0^{-\frac{\xi}{\lambda_4}} K(\lambda_4 \nu + x, \lambda_4 \nu + \xi) \Sigma^{+-}(\lambda_4 \nu + \xi) d\nu \, \Sigma^{-+}(\xi) \end{aligned} \tag{27a}$$

$$0 = K(x, x) \Lambda^+ + \Lambda^- K(x, x) + \Sigma^{-+}(x). \tag{27b}$$

and $L_{11}(x, \xi)$ is then given by

$$\begin{aligned} L_{11}(x, \xi) =& -\frac{1}{\lambda_4} K(x - \xi, 0) \Lambda^+ \bar{Q}_0 \\ & + \int_0^{-\frac{\xi}{\lambda_4}} K(\lambda_4 \nu + x, \lambda_4 \nu + \xi) \Sigma^{+-}(\lambda_4 \nu + \xi) d\nu. \end{aligned} \tag{28}$$

Moreover, $T_u^{-1}(x)$ and $T_l^{-1}(x)$ are obtained by separating the transformation (16) in two parts

$$\begin{bmatrix} T_u^{-1}(x) \\ T_l^{-1}(x) \end{bmatrix} = \begin{bmatrix} 0 & e^{-\frac{\hat{J}_{22}}{v_2^*} x} & 0 & 0 \\ 0 & 0 & e^{-\frac{\hat{J}_{33}}{\lambda_3} x} & 0 \\ e^{-\frac{\hat{J}_{11}}{v_1^*} x} & 0 & 0 & 0 \\ 0 & 0 & 0 & e^{-\frac{\hat{J}_{44}}{\lambda_4} x} \end{bmatrix} \Theta^{-1}, \tag{29}$$

where $T_u^{-1}(x) \in \mathbb{R}^{3 \times 4}$ and $T_l^{-1}(x) \in \mathbb{R}^{1 \times 4}$.

3.2. Anti-collocated boundary observer design

Next, a boundary observer design for full-state observation is proposed. In this work, an anti-collocated boundary observer is designed, i.e. the densities and velocities of both classes are measured at the opposite of the boundary where the control input acts. Therefore, it is assumed that $\bar{y}(t) = w_4(0, t)$ is known. Since $w_4(0, t)$ cannot be measured directly, it is obtained by measuring the densities $\rho_i(0, t)$ as well as velocities $v_i(0, t)$ and applying the transformation (16) afterwards. The observer states $\hat{w}_c = (\hat{w}_1, \hat{w}_2, \hat{w}_3, \hat{w}_4)^T$ are estimates of the control design model states $w_c = (w_1, w_2, w_3, w_4)^T$ and analogously $\hat{w} = (\hat{w}_1, \hat{w}_2, \hat{w}_3)^T$

represents the estimate of w. The observer equations are

$$\hat{w}_t + \Lambda^+ \hat{w}_x = \Sigma^{++}(x)\hat{w} + \Sigma^{+-}(x)\hat{w}_4 - P^+(x)(\hat{w}_4(0,t) - w_4(0,t)) \tag{30a}$$

$$\hat{w}_{4t} - \Lambda^- \hat{w}_{4x} = \Sigma^{-+}(x)\hat{w} - P_{11}^-(x)(\hat{w}_4(0,t) - w_4(0,t)) \tag{30b}$$

with the boundary conditions

$$\hat{w}(0,t) = \bar{Q}_0 w_4(0,t), \;\; \hat{w}_4(L,t) = \bar{R}_1 \hat{w}(L,t) + \bar{U}(t), \tag{31}$$

where the gains of the output injections $P^+(x)$ and $P_{11}^-(x)$ need to be designed such that the corresponding estimation error dynamics

$$\tilde{w}_t + \Lambda^+ \tilde{w}_x = \Sigma^{++}(x)\tilde{w} + \Sigma^{+-}(x)\tilde{w}_4 - P^+(x)\tilde{w}_4(0,t), \tag{32a}$$

$$\tilde{w}_{4t} - \Lambda^- \tilde{w}_{4x} = \Sigma^{-+}(x)\tilde{w} - P_{11}^-(x)\tilde{w}_4(0,t) \tag{32b}$$

with the boundary conditions

$$\tilde{w}(0,t) = 0, \tag{33a}$$

$$\tilde{w}_4(L,t) = \bar{R}_1 \tilde{w}(L,t) \tag{33b}$$

and error definitions $\tilde{w}_i(x,t) = \hat{w}_j(x,t) - w_j(x,t), \quad j = 1,\dots,4$ converge to the equilibrium at zero in a finite time. Notice that $\tilde{w} = \hat{w} - w$ and $\tilde{w}_c = \hat{w}_c - w_c$ follow according to the introduced error definition. The convergence to the equilibrium at zero in finite time is achieved by the backstepping technique. The state vector of the target system is denoted as $(\tilde{\alpha}_1, \tilde{\alpha}_2, \tilde{\alpha}_3, \tilde{\beta})^T$ with $\tilde{\alpha} = (\tilde{\alpha}_1, \tilde{\alpha}_2, \tilde{\alpha}_3)^T$ and the kernels introduced in the backstepping transformation are $M(x,\xi) = \left\{m_{j1}(x,\xi)\right\}_{1\le j\le 3}$ and $N_{11}(x,\xi)$. Thus, the backstepping transformation is given by

$$\tilde{w}(x,t) = \tilde{\alpha}(x,t) + \int_0^x M(x,\xi)\tilde{\beta}(\xi,t)d\xi, \tag{34a}$$

$$\tilde{w}_4(x,t) = \tilde{\beta}(x,t) + \int_0^x N_{11}(x,\xi)\tilde{\beta}(\xi,t)d\xi. \tag{34b}$$

The kernels $M(x,\xi)$ and $N_{11}(x,\xi)$ are defined in the triangular domain $\mathscr{T}$. In addition, the well-posed target system is defined as

$$\tilde{\alpha}_t + \Lambda^+ \tilde{\alpha}_x = \Sigma^{++}(x)\tilde{\alpha} + \int_0^x D^+(x,\xi)\tilde{\alpha}(\xi,t)d\xi, \tag{35a}$$

$$\tilde{\beta}_t - \Lambda^- \tilde{\beta}_x = \Sigma^{-+}(x)\tilde{\alpha} + \int_0^x D^-(x,\xi)\tilde{\alpha}(\xi,t)d\xi \tag{35b}$$

with the boundary conditions

$$\tilde{\alpha}(0,t) = 0, \tag{36a}$$

$$\tilde{\beta}(L,t) = \bar{R}_1 \tilde{\alpha}(L,t). \tag{36b}$$

It can be shown that the target system converges in finite time t_F, given by

$$t_F = \frac{L}{v_2^*} + \frac{L}{-\lambda_4}. \tag{37}$$

Besides, the coefficients $D^+(x,\xi) \in \mathbb{R}^{3\times 3}$ and $D^-(x,\xi) \in \mathbb{R}^{1\times 3}$ still need to be determined in the following. The kernel equations for $M(x,\xi)$ and $N_{11}(x,\xi)$ are obtained by inserting the transformation (34) as well as derivatives with respect to time and space of (34) in the PDEs of the error system (32) and noticing that $\tilde{\beta}(0,t) = \tilde{w}(0,t)$. In addition, the fourth boundary condition is deduced by evaluating (34b) at $x = L$, plugging in the corresponding boundary conditions of error system and target system, (33b) and (36b), and inserting (34a) evaluated at $x = L$ afterwards. It can be shown that the well-posedness of the kernel equations is equivalent to the one of the kernel equations for $K(x,\xi)$ and $L_{11}(x,\xi)$ by transforming them to the same structure. Similar to the full-state feedback design, solving the PDE for $N_{11}(x,\xi)$ with the method of characteristics delivers the expression

$$N_{11}(x,\xi) = \bar{R}_1 M(L, L-(x-\xi)) + \int_0^{\frac{x-L}{\lambda_4}} \Sigma^{-+}(-\lambda_4\nu + x)M(-\lambda_4\nu + x, -\lambda_4\nu + \xi)d\nu, \tag{38}$$

depending on $M(x,\xi)$. Hence, the kernel equations are reduced to three PDEs and three boundary conditions

$$0 = -\Lambda^- M_\xi(x,\xi) + \Lambda^+ M_x(x,\xi) - \Sigma^{++}(x)M(x,\xi) - \Sigma^{+-}(x)\bar{R}_1 M(L, L-(x-\xi)) - \Sigma^{+-}(x)\int_0^{\frac{x-L}{\lambda_4}} \Sigma^{-+}(x-\lambda_4\nu)M(x-\lambda_4\nu, \xi-\lambda_4\nu)d\nu, \tag{39a}$$

$$0 = M(\xi,\xi)\Lambda^- + \Lambda^+ M(\xi,\xi) - \Sigma^{+-}(\xi). \tag{39b}$$

Besides, the computation of the kernel equations yields the expressions of $D^+(x,\xi)$ and $D^-(x,\xi)$ as well as

$$P^+(x) = -\lambda_4 M(x,0), \;\; P_{11}^-(x) = -\lambda_4 N_{11}(x,0). \tag{40}$$

Thus, the observer design is completed. Employing the inverse of the transformation (16) to the estimates $\hat{w}_c$ generated by the observer yields the estimates of the density and velocity perturbations $\hat{z} = (\hat{\tilde{\rho}}_1, \hat{\tilde{v}}_1, \hat{\tilde{\rho}}_2, \hat{\tilde{v}}_2)^T$. Then, the estimates of the densities and velocities

$$\hat{\rho}_i(x,t) = \hat{\tilde{\rho}}_i(x,t) + \rho_i^*, \;\; \hat{v}_i(x,t) = \hat{\tilde{v}}_i(x,t) + v_i^* \tag{41}$$

are obtained based on $\hat{z}$.

3.3. Main result

In a final step, the full-state feedback (26) and anti-collocated observer (30) with (31) are combined resulting in an output feedback control that damps out stop-and-go traffic based on a single measurement at the inlet of the track section. Therefore, the control law is reformulated in terms of the generated estimates. This is done by replacing the densities and velocities by their estimates yielding the output feedback controller

$$U(t) = -\kappa_4 e^{\frac{j_{44}}{\lambda_4}L}\bar{R}_1 T_u^{-1}(L)\hat{z}(L,t) + \kappa_4 e^{\frac{j_{44}}{\lambda_4}L}\int_0^L \left(K(L,\xi)T_u^{-1}(\xi) + L_{11}(L,\xi)T_l^{-1}(\xi)\right)\hat{z}(\xi,t)d\xi \tag{42}$$

This main result is summarized in a theorem.

Theorem 1. *The linearized two-class AR model is given by (7) with boundary conditions (12). If the control law (42) is applied in (12c), where the estimates are generated by the anti-collocated observer (30) and (31) with (25) and the initial profiles satisfy*

$$\tilde{\rho}_1(x,0), \tilde{v}_1(x,0), \tilde{\rho}_2(x,0), \tilde{v}_2(x,0) \in \mathscr{L}^\infty([0,L]), \tag{43}$$

then the perturbations converge to the equilibrium at zero

$$\tilde{\rho}_{e,1}(x) \equiv \tilde{v}_{e,1}(x) \equiv \tilde{\rho}_{e,2}(x) \equiv \tilde{v}_{e,2}(x) \equiv 0 \tag{44}$$

in the finite time $2t_F$, where t_F is given by (37). The kernels $K(x,\xi)$ and $L_{11}(x,\xi)$ are obtained by solving the well-posed kernel Eqs. (27) as well as computing (28) afterwards and the observer gains are given by (40), where the kernels $M(x,\xi)$ represent the solution of the well-posed system of Eqs. (39) and $N_{11}(x,\xi)$ is given by (38).

The finite convergence time is $2t_F$, because the controller requires t_F to obtain correct state estimates and afterwards the

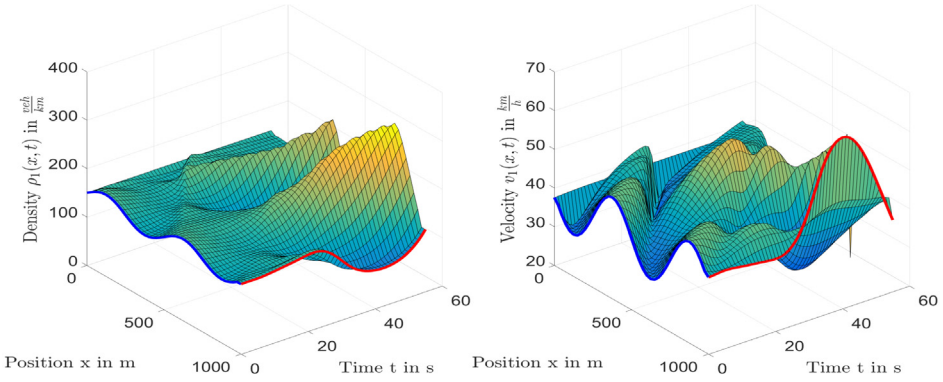

Fig. 2. Traffic density and velocity of class 1 without control.

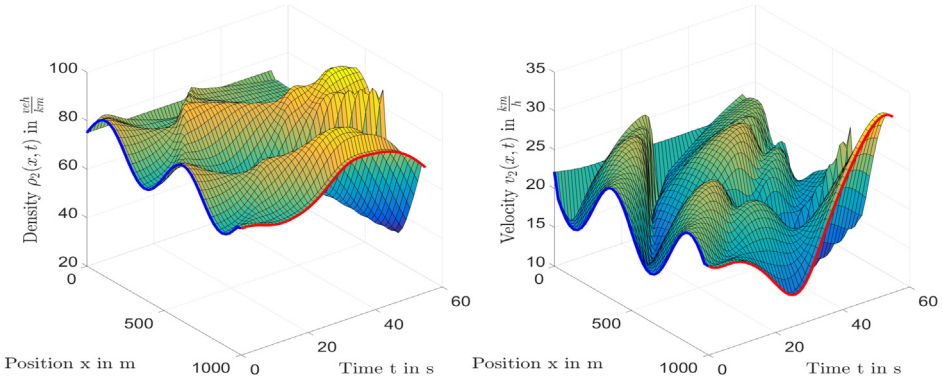

Fig. 3. Traffic density and velocity of class 2 without control.

controller needs another t_F to achieve convergence of the state variable to equilibrium state.

A statement on the stability properties of the closed loop with respect to the original problem can be made considering results on robustness like in Auriol and Meglio (2020). Therein, it is shown that the output of the closed loop system along with the controller is Input-to-State stable, see Karafyllis and Krstic (2019), if specific assumptions and conditions hold.

4. Numerical simulation

In this section, the performance of the output feedback controller is investigated by a simulation of the closed loop involving the original nonlinear model (1). First, the simulation setup and plots of the resulting densities and velocities as well as the control input are discussed. Afterwards, performance indices are computed in order to evaluate whether the output feedback controller achieves fuel savings, more comfort or a reduced total travel time.

4.1. Simulation setup and results

For the implementation, the model equations are transformed to the conservative variables ρ_1, ρ_2, $y_1 = \rho_1(v_1 - V_{e,1}(\rho_1, \rho_2))$ and $y_2 = \rho_2(v_2 - V_{e,2}(\rho_1, \rho_2))$. The update for each time step is computed in a two-stage Lax–Wendroff scheme (LeVeque, 1992). More details on applying the scheme to AR-type traffic models can be found in Yu, Gan, Bayen, and Krstic (2020). The equilibrium densities are chosen to $\rho_1^* = 150\ \frac{\text{veh}}{\text{km}}$ and $\rho_2^* = 75\ \frac{\text{veh}}{\text{km}}$ such that the investigated traffic is in the congested regime. The equilibrium velocities are determined by the choice of the equilibrium densities and result in $v_1^* \approx 38\ \frac{\text{km}}{\text{h}}$ and $v_2^* \approx 20\ \frac{\text{km}}{\text{h}}$. The initial profiles

$$\rho_i(x,0) = \rho_i^* + \frac{\rho_i^*}{8}\sin\left(\frac{4\pi}{L}x\right),\ \ v_i(x,0) = v_i^* - \frac{v_i^*}{5}\sin\left(\frac{4\pi}{L}x\right) \tag{45}$$

represent stop-and-go traffic with oscillations in density and velocity of sinusoidal shape.

The open loop simulation results are illustrated in Figs. 2 and 3. In each figure, the left plot shows the density of the corresponding vehicle class, whereas the plot on the right hand side illustrates the velocity. The values of the states at the outlet of the track section are marked with a red line, whereas the blue line emphasizes the initial profiles (45). The figures show that the oscillations in the densities and velocities do not vanish without any control input.

Figs. 4 to 5 show the simulation results for the initial profiles using the designed output feedback control. Since the observer requires t_F to estimate the states without error and afterwards the controller needs t_F to achieve finite time convergence, the total finite convergence time is $2t_F \approx 474\,\text{s}$ highlighted with a green line. The results verify that the controller achieves finite time convergence of all states $\rho_i(x,t)$ and $v_i(x,t)$ to their equilibrium values. Considering the control input in Fig. 6, it shows that $U(t)$ is continuous and nontrivial for this test case. Additionally, the control input is negative and bounded satisfying $|U(t)| < 0.25\ \frac{\text{veh}}{\text{s}}$. While taking (11b) into account, the constant total boundary flow rate is $q^* = \rho_1^* v_1^* + \rho_2^* v_2^* = 2.0242\ \frac{\text{veh}}{\text{s}}$. Furthermore, we assume that the open-loop ramp inflow $q_{in}^* = 0.4\ \frac{\text{veh}}{\text{s}}$ around 20% of the mainline flow, thus it holds that

$$q_{in}^* + U(t) > 0,\ \ \forall t \in [0, t_{sim}] \tag{46}$$

and therefore the traffic flow leaving the track section is positive.

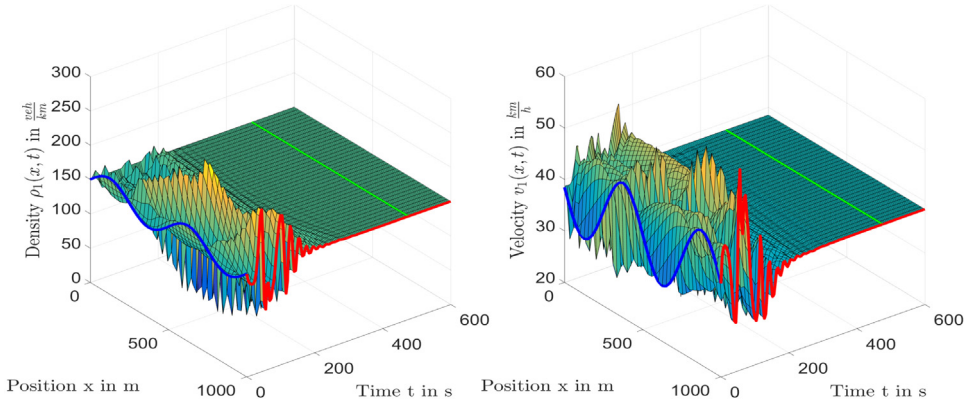

Fig. 4. Traffic density and velocity of class 1 with output feedback control. The green line indicates $2t_F$.

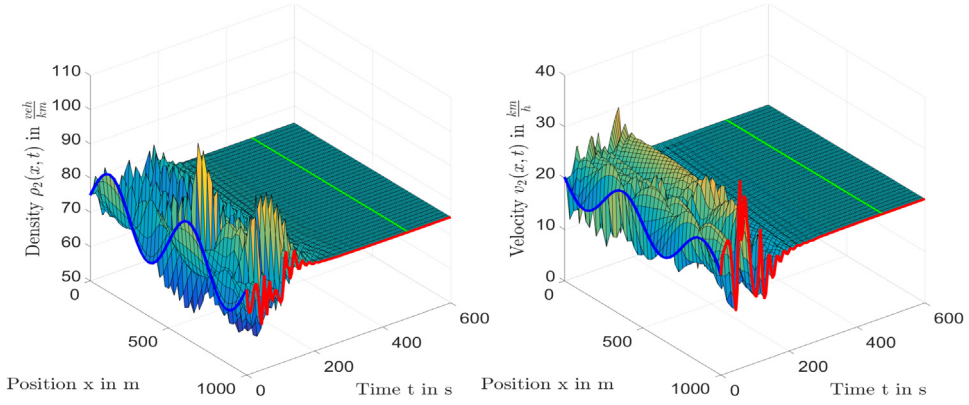

Fig. 5. Traffic density and velocity of class 2 with output feedback control. The green line indicates $2t_F$.

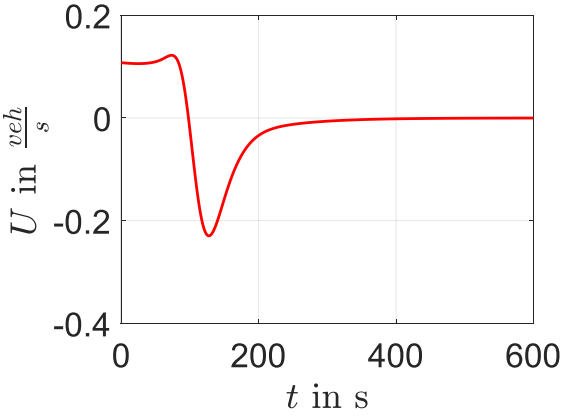

Fig. 6. Traffic flow perturbation $U(t)$ controlled by the ramp metering.

4.2. Performance indices

The considered performance indices

$$J_{fuel} = \int_0^{t_{sim}} \int_0^L \max\{0, b_0 + b_1 v(x,t) + b_2 v(x,t) a(x,t) + b_3 a^2(x,t)\} \rho(x,t)\,\mathrm{d}x\,\mathrm{d}t \tag{47a}$$

$$J_{comfort} = \int_0^{t_{sim}} \int_0^L (a(x,t)^2 + a_t(x,t)^2) \rho(x,t)\,\mathrm{d}x\,\mathrm{d}t \tag{47b}$$

$$J_{TTT} = \int_0^{t_{sim}} \int_0^L \rho(x,t)\,\mathrm{d}x\,\mathrm{d}t \tag{47c}$$

are introduced in chapter 21 of Treiber and Kesting (2013) and the fuel consumption model is adopted according to Ahn (1998) such that a crucial dependence in order to demonstrate fuel savings by damping of traffic oscillations is included. Thereby, the parameters are given by $L = 1\,\mathrm{km}$, $t_{sim} = 600\,\mathrm{s}$, $b_0 = 25 \cdot 10^{-3}\ \frac{\mathrm{l}}{\mathrm{s}}$, $b_1 = 24.5 \cdot 10^{-6}\ \frac{\mathrm{l}}{\mathrm{m}}$, $b_2 = 125 \cdot 10^{-6}\ \frac{\mathrm{ls}^2}{\mathrm{m}^2}$ and it is assumed that $b_3 = 95 \cdot 10^{-4}\ \frac{\mathrm{ls}^3}{\mathrm{m}^2}$. Notice that $a(x,t)$ is defined as the local acceleration $a(x,t) = v_t(x,t) + v(x,t)v_x(x,t)$. The performance of the controller is evaluated by computing (47) for the open loop simulation and comparing it to the values obtained by the closed loop simulation. In the following, $J_{X,OL}$ denote the performance indices with respect to the open loop results, whereas $J_{X,CL}$ denote the indices with respect to the closed loop results, where $X \in \{\text{fuel, comfort, TTT}\}$. The relative values

$$\frac{J_{fuel,CL}}{J_{fuel,OL}} = 0.9407, \quad \frac{J_{comfort,CL}}{J_{comfort,OL}} = 0.7933, \quad \frac{J_{TTT,CL}}{J_{TTT,OL}} \approx 1.0$$

indicate that the vehicles consume 5.93% less fuel, feel 20.67% more comfortable and require the same total travel time, if the controller is applied within $t_{sim} = 600\,\mathrm{s}$.

5. Concluding remarks

This paper develops an output feedback controller for the linearized two-class AR traffic PDE model. The local exponential H^2 stability result can be proved for the quasi-linear hyperbolic PDE model of this paper following Hu, Vazquez, Meglio, and Krstic (2019), but that so far a local finite-time stabilization for coupled hyperbolic PDEs has not been obtained yet in the literature. If the initial condition is far from the equilibrium profile, the finite-time

convergence is not guaranteed when the proposed controller is applied to the original system.

This work leads to further problems that will be explored in the future. First, it is typically preferred that the measurement for the observer is at the same spot where the control input acts on the system. Therefore, the design of the collocated observer is a result of great interest. In addition, the extended AR traffic model presented in Mohan and Ramadurai (2017) is formulated for n classes and there are results for $n+m$ heterodirectional behaving linear PDEs in the literature which enables the extension to more than two classes and hence even more realistic considerations.

References

Ahn, K. (1998). *Microscopic fuel consumption and emission modeling* (Ph. D. thesis), USA: Virginia Tech, https://vtechworks.lib.vt.edu/bitstream/handle/10919/36471/ETD.pdf.

Auriol, J., & Meglio, F. D. (2020). Robust output feedback stabilization for two heterodirectional hyperbolic PDEs. *Automatica*, *115*, Article 108896. http://dx.doi.org/10.1016/j.automatica.2020.108896.

Bekiaris-Liberis, N., & Delis, A. (2019). Feedback control of Freeway traffic flow via time-gap manipulation of ACC-Equipped Vehicles: A PDE-based approach. *IFAC-PapersOnLine*, *52*(6), 1–6.

Burkhardt, M., Yu, H., & Krstic, M. (2020). *Suppression of oscillations in two-class traffic by full-state feedback*. arXiv preprint arXiv:2001.01504. https://arxiv.org/pdf/2001.01504.pdf.

Deo, P., De Schutter, B., & Hegyi, A. (2009). Model predictive control for multi-class traffic flows. In *Proceedings of the 12th IFAC Symposium on Transportation Systems* (pp. 25–30).

Deutscher, J. (2017). Finite-time output regulation for linear 2 × 2 hyperbolic systems using backstepping. *Automatica*, *75*, 54–62.

Greenshields, B. D., Channing, W., & Miller, H. (1935). A study of traffic capacity. In *Highway research board proceedings, Vol. 1935*. National Research Council (USA), Highway Research Board.

Gupta, A. K., & Katiyar, V. K. (2007). A new multi-class continuum model for traffic flow. *Transportmetrica*, *3*(1), 73–85.

Hu, L., Meglio, F. D., Vazquez, R., & Krstic, M. (2015). Control of homodirectional and general heterodirectional linear coupled hyperbolic PDEs. *IEEE Transactions on Automatic Control*, *61*(11), 3301–3314.

Hu, L., Vazquez, R., Meglio, F. D., & Krstic, M. (2019). Boundary exponential stabilization of 1-dimensional inhomogeneous quasi-linear hyperbolic systems. *SIAM Journal on Control and Optimization*, *57*(2), 963–998.

Jiang, R., & Wu, Q. S. (2004). Extended speed gradient model for mixed traffic. *Transportation Research Record*, *1883*(1), 78–84.

Karafyllis, I., Bekiaris-Liberis, N., & Papageorgiou, Markos (2019). Feedback control of nonlinear hyperbolic PDE systems inspired by traffic flow models. *IEEE Transactions on Automatic Control*, *64*(9), 3647–3662.

Karafyllis, I., & Krstic, M. (2019). *Input-to-state stability for PDEs*. Springer International Publishing, http://dx.doi.org/10.1007/978-3-319-91011-6.

LeVeque, R. J. (1992). *Numerical methods for conservation laws, Vol. 3* (p. 125). Basel: Birkhäuser, http://dx.doi.org/10.1007/978-3-0348-5116-9.

Liu, S., Hellendoorn, H., & De Schutter, B. (2017). Model predictive control for freeway networks based on multi-class Traffic Flow and Emission Models. *IEEE Transactions on Intelligent Transportation Systems*, *18*(2), 306–320.

Logghe, S. (2003). *Dynamic modeling of heterogeneous vehicular traffic* (Ph. D. thesis), Belgium: Katholieke Universiteit Leuven, Link: https://www.mech.kuleuven.be/cib/verkeer/dwn/pub/P2003B.pdf.

Mallikarjuna, C., & Rao, K. R. (2006). Area occupancy characteristics of heterogeneous traffic. *Transportmetrica*, *2*(3), 223–236.

Meglio, F. D., Vazquez, R., & Krstic, M. (2013). Stabilization of a system of $n+1$ coupled first-order hyperbolic linear PDEs with a single boundary input. *IEEE Transactions on Automatic Control*, *58*(12), 3097–3111.

Mohan, R., & Ramadurai, G. (2017). Heterogeneous traffic flow modelling using second-order macroscopic continuum model. *Physics Letters. A*, *381*(3), 115–123.

Pasquale, C., Papamichail, I., Roncoli, C., Sacone, S., Siri, S., & Papageorgiou, M. (2015). Two-class freeway traffic regulation to reduce congestion and emissions via nonlinear optimal control. *Transportation Research C: Emerging Technologies*, *55*, 85–99.

Su, L., Wang, J. M., & Krstic, M. (2017). Boundary feedback stabilization of a class of coupled hyperbolic equations with nonlocal terms. *IEEE Transactions on Automatic Control*, *63*(8), 2633–2640.

Tang, T. Q., Huang, H. J., Zhao, S. G., & Shang, H. Y. (2009). A new dynamic model for heterogeneous traffic flow. *Physics Letters. A*, *373*(29), 2461–2466.

Tang, C. F., Jiang, R., Wu, Q. S., Wiwatanapataphee, B., & Wu, Y. H. (2007). Mixed traffic flow in anisotropic continuum model. *Transportation Research Record*, *1999*(1), 13–22.

Treiber, M., & Kesting, A. (2013). *Traffic flow dynamics: Data, models and simulation*. Springer-Verlag Berlin Heidelberg, http://dx.doi.org/10.1007/978-3-642-32460-4.

Yu, H., Gan, Q., Bayen, A., & Krstic, M. (2020). PDE traffic observer validated on freeway data. *IEEE Transactions on Control Systems Technology*, http://dx.doi.org/10.1109/TCST.2020.2989101.

Yu, H., & Krstic, M. (2018). Varying speed limit control of Aw-Rascle-Zhang traffic model. In *2018 21st international conference on intelligent transportation systems (ITSC)* (pp. 1846–1851).

Yu, H., & Krstic, M. (2019). Traffic congestion control for Aw-Rascle-Zhang model. *Automatica*, *100*, 38–51.

Zhang, P., Liu, R. X., Wong, S. C., & Dai, S. Q. (2006). Hyperbolicity and kinematic waves of a class of multi-population partial differential equations. *European Journal of Applied Mathematics*, *17*(2), 171–200.

Zhang, L., & Prieur, C. (2017). Necessary and sufficient conditions on the exponential stability of positive hyperbolic systems. *IEEE Transactions on Automatic Control*, *62*(7), 3610–3617.

Mark Burkhardt received his B.S. degree in Engineering Cybernetics at the University of Stuttgart, Germany. After pursuing research as a Visiting Graduate Student at the University of California, San Diego, USA, he completed the consecutive M.S. degree in Engineering Cybernetics. Currently, he is working as a Ph.D. student at the Institute for System Dynamics at the University of Stuttgart. His research focusses on the control of large-scale robotic systems and the development of a cyber–physical construction platform for automated load handling.

Huan Yu received her B.S. degree in Aerospace Engineering from Northwestern Polytechnical University, China in 2013 and the M.S. and Ph.D. degree in Mechanical and Aerospace Engineering from University of California, San Diego in 2015 and 2019. She was a visiting researcher at University of California, Berkeley in 2018 and Massachusetts Institute of Technology in 2019. She is currently a postdoc researcher at University of California, San Diego. Her research focuses on the control and estimation of distributed parameter system, intelligent transportation system, reinforcement learning, extremum seeking.

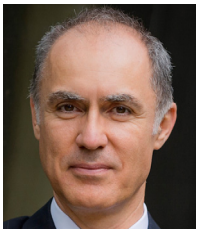

Miroslav Krstic is Distinguished Professor of Mechanical and Aerospace Engineering, holds the Alspach endowed chair, and is the founding director of the Cymer Center for Control Systems and Dynamics at UC San Diego. He also serves as Senior Associate Vice Chancellor for Research at UCSD. As a graduate student, Krstic won the UC Santa Barbara best dissertation award and student best paper awards at CDC and ACC. Krstic has been elected Fellow of seven scientific societies – IEEE, IFAC, ASME, SIAM, AAAS, IET (UK), and AIAA (Assoc. Fellow) – and as a foreign member of the Serbian Academy of Sciences and Arts and of the Academy of Engineering of Serbia. He has received the SIAM Reid Prize, ASME Oldenburger Medal, Nyquist Lecture Prize, Paynter Outstanding Investigator Award, Ragazzini Education Award, IFAC Nonlinear Control Systems Award, Chestnut textbook prize, Control Systems Society Distinguished Member Award, the PECASE, NSF Career, and ONR Young Investigator awards, the Schuck ('96 and '19) and Axelby paper prizes, and the first UCSD Research Award given to an engineer. Krstic has also been awarded the Springer Visiting Professorship at UC Berkeley, the Distinguished Visiting Fellowship of the Royal Academy of Engineering, the Invitation Fellowship of the Japan Society for the Promotion of Science, and four honorary professorships outside of the United States. He serves as Editor-in-Chief of Systems & Control Letters and has been serving as Senior Editor in Automatica and IEEE Transactions on Automatic Control, as editor of two Springer book series, and has served as Vice President for Technical Activities of the IEEE Control Systems Society and as chair of the IEEE CSS Fellow Committee. Krstic has coauthored fifteen books on adaptive, nonlinear, and stochastic control, extremum seeking, control of PDE systems including turbulent flows, and control of delay systems.